Chapter 3

Overview of the experiment

3.1 Guiding design principles

Historically, neutrino oscillation experiments have turned out to be quite difficult. Evidence for neutrino oscillations has been tentatively reported on several occasions only to be retracted or modified later. The skepticism that exists, at least in some circles, regarding the definitiveness of the LSND results[1] illustrates the point that the standards for a convincing experiment in this area are very high.

In designing the MINOS experiment we have paid close attention to these factors[2, 3]. Accordingly, our goal is to be able to perform several independent and parallel measurements, each one of which by itself is capable of addressing the question of neutrino oscillations. Thus we should be able to obtain internal verification of any effect that we might observe. That is, to be believable, our experiment should yield several independent measurements which give a consistent picture of the oscillation scenario.

Very briefly, the physics goals of MINOS are:

a) If Nature has chosen not to have neutrino oscillations in the parameter space accessible to MINOS, we want to be able to demonstrate this fact convincingly over as large an area in oscillation parameter space as possible.

b) If oscillations do exist in the space accessible to MINOS, we want to convincingly demonstrate their existence, measure the oscillation parameters with high precision, and determine the oscillation modes. Specifically, we want to ensure that we can cover the full region of parameter space suggested by the Super-Kamiokande experiment.

These broad physics goals determine the general design of the experiment. To reduce systematic uncertainties as much as possible, we believe that it is necessary to have two detectors: one close to the neutrino source, i.e. on the Fermilab site, and the other one far away, so that the oscillations have sufficient time to develop, even for low Δm^2. The neutrino beam spectra at the two locations should be as nearly identical as possible and their difference should be well understood and independently verifiable. Similarly, the two detectors should be as similar as possible in their important parameters, namely the nature of the active detector, the steel thickness, and the magnetic field configuration in the neutrino interaction

regions. The beam and detector similarities should minimize the systematic errors in the comparison of results from the two detectors. Because the statistical significance of the results will be determined by the event rate in the far detector, we can sacrifice statistics at the near detector to make the conditions there as similar as possible to those at the far detector.

Neutrino oscillations can cause changes in the neutrino event rate in the far detector, as extrapolated from observations in the near detector; oscillations can also cause differences in the characteristics of the events observed in the two detectors. The systematics of these two kinds of measurements will be quite different. Thus, following our goal of having as diverse a set of measurements as possible, we plan to compare both the rates and the characteristics of events in the two detectors.

An additional experimental feature we have incorporated into the design of MINOS is the ability to change experimental conditions in response to the initial results from the experiment. Results obtained in the modified experiment should be different in a way that is predictable from the hypothesis purporting to explain the initial results. Thus, for example, we can change the tune and/or the arrangement of the wide-band beam horn system in order to change the neutrino energy spectrum. Alternatively, we might switch to the narrow-band beam mode in response to the initial results, so as to increase or decrease the size of the observed effect in a predictable way.

Finally, we want to be responsive to the fourth recommendation of the Sciulli Subpanel[4], namely to maintain as much flexibility as feasible to respond to future physics and technology developments[5]. In that spirit, we have recently developed alternative beam configurations which shift the neutrino spectra to lower energies. Such beams could be more appropriate for investigating oscillations with Δm^2 around 10^{-3} eV^2. Our detector design has also been chosen with the goal of maintaining flexibility; for example, the scintillator active detector and the relatively thin steel absorber planes allow us to extend our sensitivity for detecting and identifying oscillations down to relatively low energies[6]. This detector design will also allow us to perform independent atmospheric neutrino flux measurements. Such measurements might be quite topical even 5 to 10 years from now if the results from accelerator neutrinos and atmospheric neutrinos do not appear to have a single self-consistent explanation. We are also proceeding in parallel on an R&D effort for a possible emulsion detector (see Chapter 11) in the ECC (emulsion cloud chamber) mode, to be used as a potential complementary τ-lepton detector.

3.2 Summary of experiment goals and requirements

This Section gives a brief summary of the specific physics goals of the MINOS experiment and the properties of the detectors which we have designed to reach these goals. The physics goals and the rationale for them are discussed in more detail in Section 3.7 and in Reference [3].

As discussed in the preceding Section, the general goals of the experiment are to extend the search for neutrino oscillations into previously unexplored regions of Δm^2 and $\sin^2(2\theta)$ parameter space. If oscillations are found, the experiment should be able to measure the parameters and to identify the oscillation modes. The basic experimental parameters have been chosen to have maximum sensitivity to $\nu_\mu \rightarrow \nu_\tau$ and $\nu_\mu \rightarrow \nu_e$ oscillations in the region

of parameter space suggested by the atmospheric neutrino anomaly observed by Super-Kamiokande and other experiments. The determination of oscillation parameters can be made with a precision comparable to the limits achieved by ν_e disappearance experiments at reactors. If one oscillation mode (e.g., $\nu_\mu \to \nu_\tau$) is dominant, a limit on the admixture of the other mode (e.g., $\nu_\mu \to \nu_e$) can be set at better than 10% to provide a good test of models which predict equal oscillation strengths. The ability to identify τ lepton decays explicitly should give a statistically compelling signal if the atmospheric neutrino anomaly is caused by $\nu_\mu \to \nu_\tau$ oscillations, as suggested by Super-Kamiokande results. Table 3.1 gives a quantitative summary of the physics goals which are achieved by the MINOS baseline design.

Measurement	Sensitivity (90% CL)
$\nu_\mu \to \nu_\tau$ limit, high Δm^2	$\sin^2(2\theta) > 1.9 \times 10^{-2}$ (NC/CC test)
$\nu_\mu \to \nu_\tau$ limit, $\sin^2(2\theta) = 1$, high energy beam	$\Delta m^2 > 2 \times 10^{-3}$ eV^2 (NC/CC test)
$\nu_\mu \to \nu_\tau$ limit, $\sin^2(2\theta) = 1$, low energy beam	$\Delta m^2 > 6 \times 10^{-4}$ eV^2 (ν_μ disappearance)
$\nu_\mu \to \nu_\tau$ limit, $\sin^2(2\theta) = 1$, τ identification	$\Delta m^2 > 1.7 \times 10^{-3}$ eV^2 (ν_τ CC events)
$\nu_\mu \to \nu_e$ limit, high Δm^2	$\sin^2(2\theta) > 2 \times 10^{-3}$ (ν_e appearance test)
$\nu_\mu \to \nu_e$ limit, $\sin^2(2\theta) = 1$	$\Delta m^2 > 3 \times 10^{-4}$ eV^2 (ν_e appearance test)
Δm^2 measurement precision	1×10^{-3} eV^2 for $\Delta m^2 = 10^{-2}$ eV^2
$\sin^2(2\theta)$ measurement precision	1×10^{-1} for $\Delta m^2 = 10^{-2}$ eV^2
Limit on admixture of $\nu_\mu \to \nu_e$, $\nu_\mu \to \nu_\tau$	$\sin^2(2\theta) < 0.06$ for $\Delta m^2 = 10^{-2}$ eV^2

Table 3.1: MINOS physics goals. The baseline detector described in this report will achieve these sensitivities in a two year run. The high energy wide-band (PH2) beam is assumed unless otherwise indicated. A beam optimized for lower energy neutrinos extends these sensitivities to lower values of Δm^2. If oscillations are not found, the 90% confidence level limits shown will be achieved. If oscillations are observed with $\Delta m^2 = 10^{-2}$ eV^2, the parameters and modes will be determined with the indicated precisions.

The goals discussed above were used to determine the detector and neutrino beam parameters of our baseline design. The high energy configuration of the wide band beam is well above threshold for charged current ν_τ interactions; this energy, together with the far detector distance and mass, gives Δm^2 and $\sin^2(2\theta)$ sensitivities over a large fraction of the region suggested by the atmospheric neutrino anomaly. The lower end of the region suggested by the Super-Kamiokande experiment can be explored with the low energy beam option. The most sensitive limits on the occurrence of $\nu_\mu \to \nu_\tau$ oscillations are set by comparing the ratio of charged current to neutral current events in the near and far detectors. Thus the beam spectra should be as similar as possible at the two detectors and the detectors themselves should be very similar. The statistical limits on sensitivity to oscillations are set by the far detector mass. The steel must be thin enough to give good efficiency for neutral current events with small visible hadronic energies. The near detector must be located far enough downstream from the decay pipe that the beam energy spectrum is as close as possible to that at the far detector. The active detector technology needs to be effective for both detectors, i.e., appropriate for both the large neutrino flux at the near detector and also for the much lower flux at the far detector.

If oscillations occur, the experiment must be able to measure the parameters and distinguish between different oscillation modes. This requires good energy resolution for hadrons, muons and electrons, and the ability to distinguish the topologies of ν_μ, ν_e, and ν_τ interactions. These requirements determine the transverse and longitudinal granularities and the magnetic field strength; however, sensitivities depend rather weakly on these parameters. Calibration of the relative energy scales of the near and far detectors is important for the determination of Δm^2. Good hadronic energy resolution is also important for this measurement; good electromagnetic energy resolution is needed for ν_e identification and parameter measurement if $\nu_\mu \rightarrow \nu_e$ oscillations occur. The explicit identification of the decays of τ leptons from ν_τ charged current interactions, via statistical analyses, puts stringent demands on several detector parameters: longitudinal and transverse granularities, π^o/electron identification and the tails of the calorimetric energy response. The baseline design has compromised on these τ-identification requirements somewhat in order to maintain a high far detector mass (for oscillation search sensitivity) while conforming to overall cost guidelines. However, our design is quite conservative with regard to Δm^2 sensitivity: we have chosen detector parameters which will retain good event identification and measurement capabilities should it turn out to be advisable, for physics reasons, to run at lower beam energies than the high-energy wide-band beam. Table 3.2 summarizes the experimental parameters of the MINOS baseline design.

Parameter	Value
Near detector mass	0.98 (metric) kt total, 0.1 kt fiducial
Far detector mass (2 supermodules)	5.4 (metric) kt total, 3.3 kt fiducial
Steel planes (far detector)	8-m wide, 2.54-cm thick octagons
Magnetic field (far detector)	Toroidal, 1.5 T at 2 m radius
Active detector planes	Extruded polystyrene scintillator strips
Active detector strips	4.1-cm wide, 1-cm thick, ~8-m long
Near detector distance from decay pipe	290 m
Far detector distance from decay pipe	730 km
Cosmic ray rates	270 Hz in near det., 1 Hz in far det.
Neutrino energy range (3 configurations)	1 to 25 GeV
Detector energy scale calibration	5% absolute, 2% near-far
Detector EM energy resolution	$23\%/\sqrt{E}$ (<5% constant term)
Detector hadron energy resolution	$60\%/\sqrt{E}$ (<7% constant term)
Detector muon energy resolution	<12% (from curvature or range)
NC-CC event separation	Efficiency >90%, correctable to 99.5%
Electron/π separation	Hadron rejection $\sim 10^3$ for $\epsilon_e \sim$20%
Far det. ν event rate (high-energy beam)	3000 ν_μ CC events/kt/yr (no oscillations)
Near det. ν event rate (high-energy beam)	20 events/spill in target region
Near-far relative rate uncertainty	2%

Table 3.2: MINOS experimental parameters with the wide-band (PH2) beam.

3.3 Geographical layout of the experiment

The "map" of the experiment is illustrated in Figure 3.1. The neutrino beam is produced by the 120 GeV protons from the Fermilab Main Injector and is aimed at the Soudan mine in northern Minnesota, some 730 km away. Because of the earth's curvature the parent hadron beam has to be pointed downward at an angle of 57 mrad.

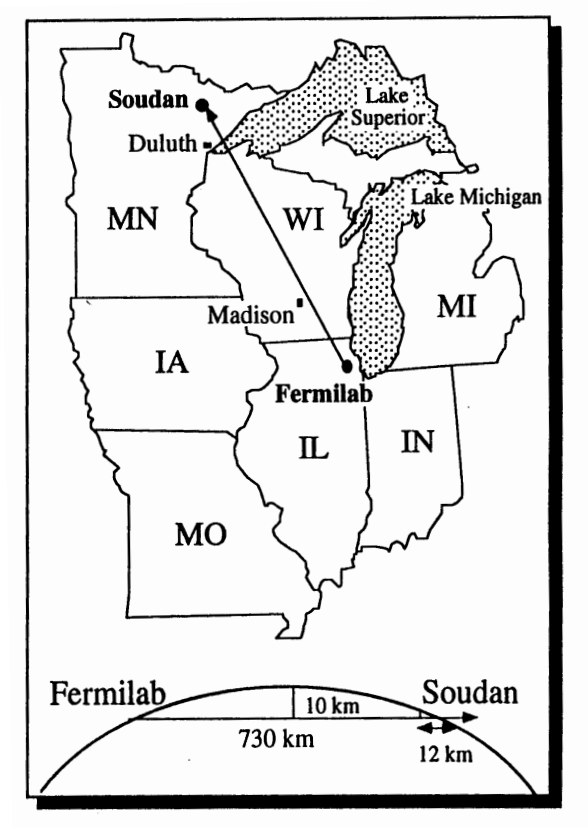

Figure 3.1: The trajectory of the MINOS neutrino beam between Fermilab and Soudan. The beam must be aimed into the earth at an angle of 57 mrad to reach Minnesota.

The hadron beam decay pipe will be 675 m long, a compromise between our desire to obtain the maximum number of π and K decays and the cost of the civil construction. The near detector is located 290 m downstream of the hadron beam absorber. This location is also a compromise between the desire to have the neutrino spectrum be as similar as possible at the two locations (arguing for a large distance) and the need to keep the construction costs low (arguing for a short distance, mainly because of the cost of constructing the near-detector cavern deep underground). The proposed layout of the MINOS experiment on the Fermilab site is shown in Figure 3.2.

The far detector will be located in the Soudan mine in northern Minnesota. This historic iron mine no longer supports active mining, but was converted some time ago into a Minnesota State Park. The MINOS detector will be constructed 710 m below ground level, in a new cavern to be excavated during 1999-2000. The axis of the MINOS cavern will point toward Fermilab; the new cavern will be constructed next to the existing underground laboratory which houses the operating Soudan 2 detector[7].

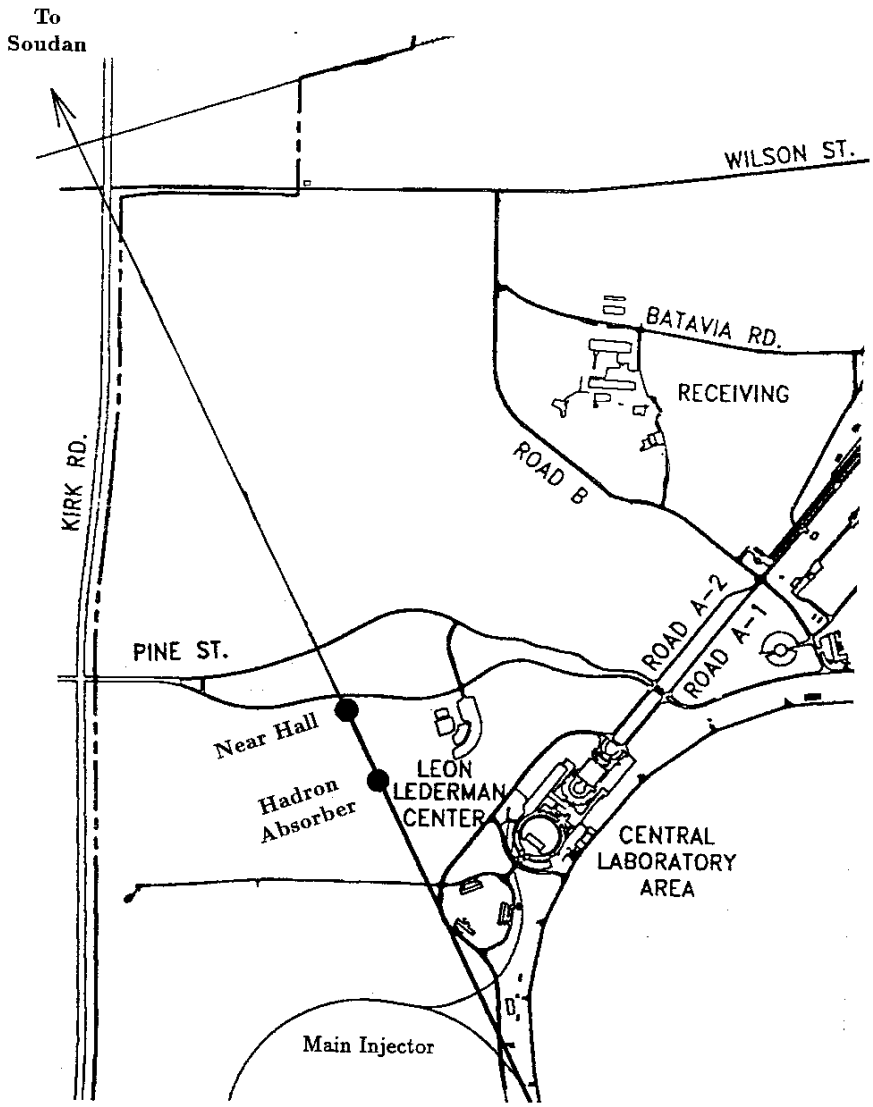

Figure 3.2: Map of the Fermilab site, showing the NuMI beamline and the approximate locations of the hadron absorber and the MINOS near hall.

Several arguments led us to the choice of the Soudan location for the MINOS far detector:

a) 730 km is a reasonable compromise between sensitivity in $\sin^2(2\theta)$, which improves as the distance L between the two detectors decreases (because of the higher event rate), and the sensitivity in Δm^2, which improves with the larger L (because low Δm^2 oscillations have more time to develop). At this distance, we can achieve sensitivities below 0.001 eV^2 in Δm^2 (with the low energy beam option) and 0.01 in $\sin^2(2\theta)$.

b) The existing infrastructure in the Soudan mine (because of its continuing use as a State Park) and the record of excellent collaboration with the state of Minnesota in carrying out the Soudan 1 and Soudan 2 experiments, has convinced us that the conditions for the MINOS experiment at Soudan will be very favorable.

c) The existing Soudan 2 detector, currently operating in the Soudan underground laboratory, will provide an additional, very fine grained, 1 kt detector whose systematics will be significantly different from those of the principal MINOS detector.

d) A distance much longer than 730 km would necessitate a steeper tunnel resulting in a higher civil construction cost at Fermilab.

e) The NuMI neutrino beamline pointing towards Soudan can be readily accommodated on the Fermilab site.

f) There are significant advantages to locating the far detector underground. These have mainly to do with a lower cosmic ray background rate and the ability to perform additional nonaccelerator measurements such as the study of high energy atmospheric neutrinos.

3.4 The neutrino beam

The NuMI neutrino beam has been described in some detail already[8, 9]. Accordingly, we focus here only on its salient features which are most relevant to the physics capabilities of the MINOS experiment.

The primary 120 GeV protons are extracted from the Main Injector using the standard resonant extraction technique over a time period of 1 msec. They are subsequently transported to the downstream target hall and aimed downwards at 3.3° so as to point at the MINOS far detector on the lowest level of the Soudan mine. By 2002 the Main Injector is expected to deliver about 4×10^{13} protons per pulse on target.

The target design optimizes neutrino yield but also takes into account the need to have a conservative design that can withstand the proton beam intensities contemplated. The target is a small diameter (matched to the transverse size of the proton beam) segmented graphite or beryllium cylinder about 160 cm long. The gaps between the segments allow most of the produced pions and kaons to leave the target before interacting. A 0° targeting angle will be used for the wide-band beam (WBB) configurations considered here.

The resulting hadron beam is subsequently sign selected and focused by specially designed focusing elements and then transported through an evacuated decay pipe, 1 m in radius and

675 m long, before striking a secondary hadron absorber downstream. Including the 50 m distance between the production target and the decay pipe, the total decay length is 725 m. The dolomite between the hadron absorber and the first MINOS detector provides sufficient shielding to range out all the muons produced by π and K decays in the beam pipe.

Our original beam design (referred to as H66) used three magnetic horns as focusing elements. The design maximized the total neutrino event rate in the far detector by optimizing the acceptance for neutrinos in the range of 8 to 25 GeV. The recent Super-Kamiokande results indicate the potential importance of achieving good sensitivity for investigation of the low Δm^2 region, necessitating a low energy beam option. With that in mind, we have developed an alternative wide-band beam design (generically referred to as PH2)[9] with two movable parabolic horns which can be configured to provide much higher fluxes at low energies than the original H66 beam. Beams optimized for investigations of different ranges of Δm^2 (and hence having maximum neutrino flux at different energies) can be obtained by varying the currents and locations of the two horns. The high energy configuration of the PH2 beam gives an energy spectrum comparable to that of the H66 beam with only slightly lower neutrino flux.

Figure 3.3 displays the calculated performance of this parabolic horn NuMI beam. The upper curve, corresponding to perfect focus and a 675 m long decay pipe, shows the maximum neutrino flux theoretically available, given the Main Injector proton intensity and the proposed NuMI target. The lower three curves show the event rate as a function of energy for three different configurations of the beam. About 3000 ν_μ CC events/kt/year are expected in the MINOS far detector for the highest energy configuration.

We have also studied the design of a narrow-band beam (NBB) for MINOS. An NBB accepts only a narrow hadron energy band and thus yields a relatively narrow energy spectrum of neutrinos, at the expense of total flux. Oscillation effects could then be easily varied by altering the choice of the central energy. In addition, such an NBB would allow identification of $\tau \rightarrow \mu\nu\nu$ decays on an event by event basis, by observation of the missing energy which is carried off by the two decay neutrinos. The design work to date gives us confidence that a beam of such a design could be constructed within the constraints imposed by the NuMI civil construction baseline design[9], although the NBB option is not included in the scope of this baseline design.

3.5 The near detector

The primary function of the near detector is to serve as a reference for the principal MINOS (far) detector in the Soudan mine. Our philosophy is to obtain a direct measurement of the rates and characteristics of the neutrino interactions before the neutrinos have had a chance to oscillate. The measurements can then be compared with the equivalent measurements at the far detector to see if oscillations have occurred. The dependence on Monte Carlo calculations is greatly reduced by comparing far detector data to near detector data instead of making comparisons to Monte Carlo predictions. For such a comparison to be most useful, the beam and detector characteristics at the two locations, as well as the experimental environment, have to be as similar as possible and their differences well understood.

There are several differences, however, that cannot be eliminated:

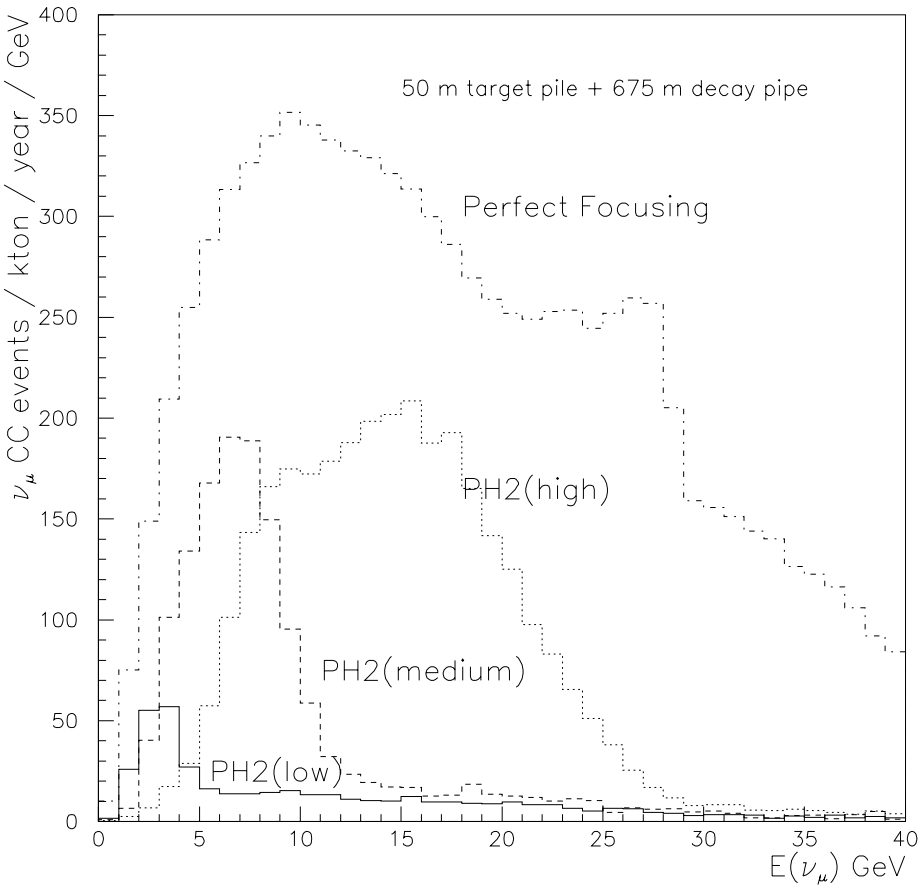

Figure 3.3: Neutrino interaction energy spectra predicted for different beam focusing conditions. 'Perfect Focusing' assumes all secondary charged particles (with the proper sign) from the target are focused into a pencil beam with no divergence. 'PH2(high),' 'PH2(medium)' and 'PH2(low)' are the high, medium and low energy configurations of the parabolic horn beam.

a) The neutrino energy spectrum at the two locations will be somewhat different. This is due to the finite length of the neutrino source. This length is comparable to the distance between a typical π or K decay point and the near detector.

b) The neutrino flux is significantly higher at the near detector.

c) The near detector is at a shallower depth than the far detector.

The beam spectra differences are due to π and K decay kinematics (a neutrino emitted at a larger angle has lower energy) and the fact that lower energy neutrinos tend to be produced further upstream (due to shorter parent lifetime). Thus the differences are easily understood. In addition, if we use neutrino events from only the central beam region of the near detector (we plan to use r $<$ 25 cm), the differences are minimized.

Flux differences at the two locations are not a problem if pileup and overlap rates are kept low, as is the case in our experiment (see Chapter 6).

Finally, the near and far detectors have different cosmic ray rates because of their different depths. Although the ratio of rates is quite large, the absolute rates at both locations are still quite low ($1.8 \times 10^{-3}/\mathrm{m}^2/\mathrm{s}$ at Soudan and $1.6\ /\mathrm{m}^2/\mathrm{s}$ in the near detector cavern). The low beam duty cycle, $<10^{-3}$, reduces the impact of cosmic rays even further and allows a very accurate measurement of the effect of any residual cosmic ray background.

The design of the near detector attempts to emulate that of the far detector in all relevant properties: the nature and thickness of absorber planes, the nature and granularity of the active detector, and the strength of the magnetic field. The basic near-detector shape is an elongated octagon, 3.8 m high and 4.8 m wide, as shown in Figure 3.4. The coil hole is placed off center horizontally, and the detector itself is positioned so that the central part of the neutrino beam is about 1 m away from the hole. This geometry was chosen to minimize the amount of steel used while still providing a sufficient steel plane area with an adequate magnetic field in the neutrino interaction region.

In the longitudinal dimension, the detector is composed of four functionally different components. Starting from the upstream end, they are:

a) **Veto part.** This is the upstream part of the detector whose neutrino interactions are not used, because of possible end effects and the need to assure that there is no background from neutron interactions. The veto part also assures that the following target region has no anomalous end effects. This part has a thickness of 0.5 m of steel.

b) **Target part.** Neutrino interactions in this part are used for the near/far comparison. It has a thickness of 1.0 m of steel.

c) **Hadron shower part.** This part has to be long enough to contain the full showers of all neutrino interactions occurring in the target part. It has a thickness of 1.5 m of steel.

d) **Muon spectrometer part.** This part is used to range out muons and/or measure their momentum by curvature. The length is determined by the momentum accuracy needed to match that of the far detector; 4 m of steel is sufficient for this.

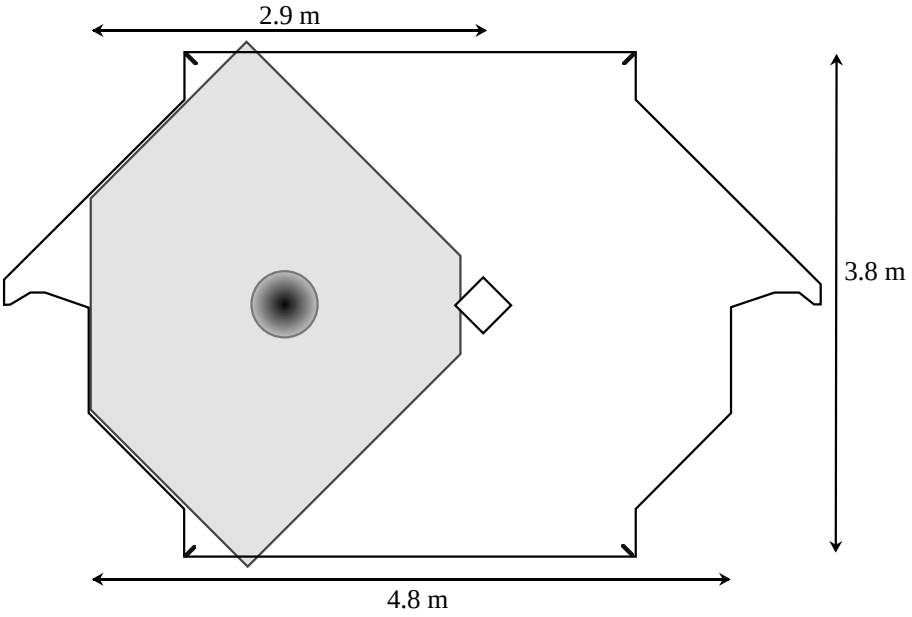

Figure 3.4: Sketch of a partially instrumented near detector plane in one of the three upstream sections, showing the area instrumented with scintillator strips. The central square represents the magnet coil hole and the circle shows the 25 cm radius central beam region. The shaded area is covered with scintillator strips and the rest of the steel plate is uncovered. Each strip is read out from its outer end only.

Figure 3.5 shows a schematic of the layout of the near detector in the longitudinal direction. The first three parts, although functionally different, are identical in the active detector technology used and their transverse and longitudinal granularities. They are also identical to the far detector in these respects. Because the accuracy of muon measurement by curvature is determined by Coulomb scattering in steel (for sufficiently long traversals, as is the case here), the requirements on the detector elements in the muon spectrometer are less stringent than in the three upstream parts. We therefore use active detectors only on every fourth plane of steel in this part.

As mentioned above, we plan to use only the central part of the neutrino beam ($r < 25$ cm) for the near/far comparison. Because the transverse spread of a hadronic shower is about half a meter at our energies and in our detector, we need to instrument only a part of the area of the upstream sections of the near detector. In order to measure the neutrino spectrum out to about 1 m from the axis, we will instrument an area of 2.8 m by 2.8 m in this region. In addition, every fifth scintillator plane in the first three sections will have a larger instrumented area to indicate the presence of tracks and interactions outside the central beam area.

The instrumentation of the near detector is very similar to that of the far detector; the basic detector elements are 4-cm wide scintillator strips with a wavelength shifting fiber imbedded in them (see Chapter 5). Because of the higher rates and the smaller number of channels, we will read out each scintillator strip in the three upstream sections separately, without the multiplexing scheme used in the far detector (see Section 3.6 below). Most

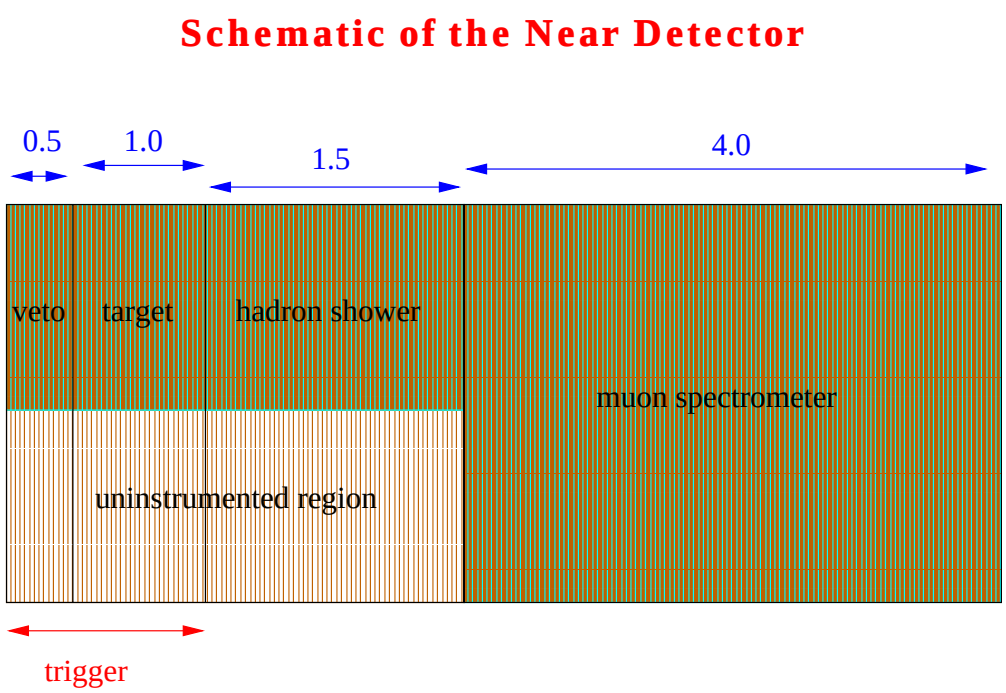

Figure 3.5: Schematic representation of the four functional parts of the MINOS near detector. The thicknesses shown (in meters) are only for the steel planes, and do not include the space occupied by detector planes. The beam enters from the left and is centered on the shaded region. Shading is used to indicate instrumented regions of the detector.

scintillator planes in the upstream part of the detector cover only about one quarter of the steel plane area, as indicated in Figure 3.4. The length of the strips is variable, corresponding to the shape of the iron, and ranges from 1.5 to 2.7 m in length. In the muon spectrometer part, the full area of the steel planes is covered with scintillator and $4\times$ multiplexed readout is used. All near detector strips are read out from only one end and the orientation of strips alternates in successive planes.

Although the rates in the near detector are considerably higher than in the far detector, they do not introduce any significant dead time, pileup, or event overlap problems (see Chapter 6). The singles rate in the detector comes mainly from the neutrino interactions in the detector and from the muons produced by the neutrinos interacting in the earth shield upstream. The neutrino event rate in the detector is shown in Figure 3.6, and the rate of muons from both sources in Figure 3.7. The contribution from hadrons and electromagnetic showers generated in neutrino interactions is shown in Figure 3.8. Because of the high probability of having more than one hit per strip from the same interaction, we plot the last rate as number of strips hit/plane/spill. From these rates we can see that even with a very conservative resolution time of 50 ns, the event overlap probability, as well as the random occupancy probability of any single strip, is considerably less than 10^{-3}.

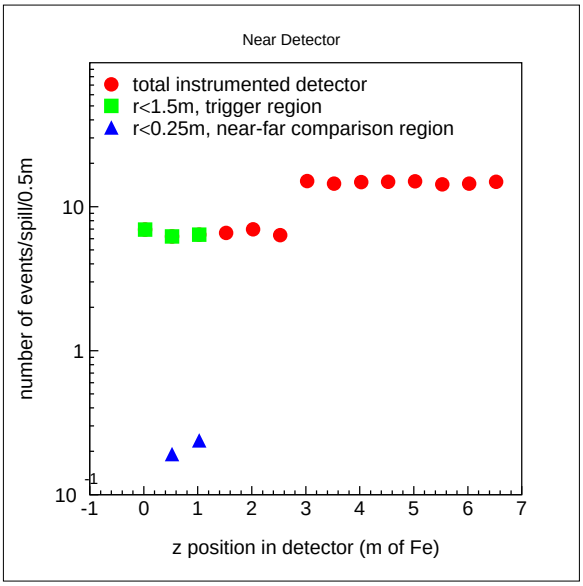

Figure 3.6: Neutrino interaction event rate in the MINOS near detector.

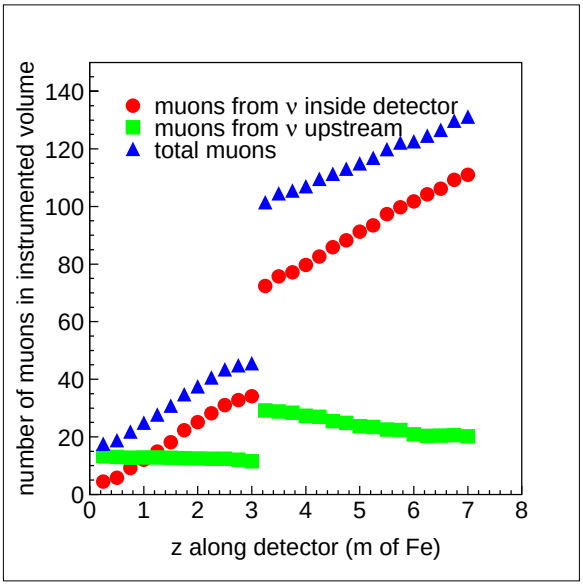

Figure 3.7: Number of muons per spill in the near detector.

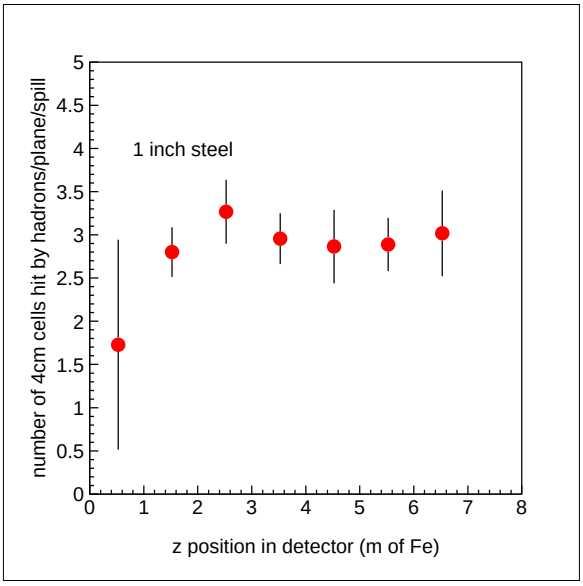

Figure 3.8: Rate contributions from hadron and electromagnetic showers in the MINOS near detector.

3.6 The far detector

The MINOS far detector is a 5.4 metric kt magnetized iron calorimeter with scintillator as the active detector. The basic module is an 8 m diameter, 1-inch thick steel plane (Chapter 4), followed by a scintillator plane (Chapter 5). A MINOS supermodule is made up of 242 of these modules (a supermodule has steel planes on both ends, so each has 242 scintillator planes and 243 steel planes); two supermodules compose the baseline MINOS far detector. Each supermodule is energized independently by current in a 15 kA-turn coil so as to provide a magnetic field in the iron averaging about 1.5 T (Chapter 4). An artist's sketch of the far detector is shown in Figure 3.9.

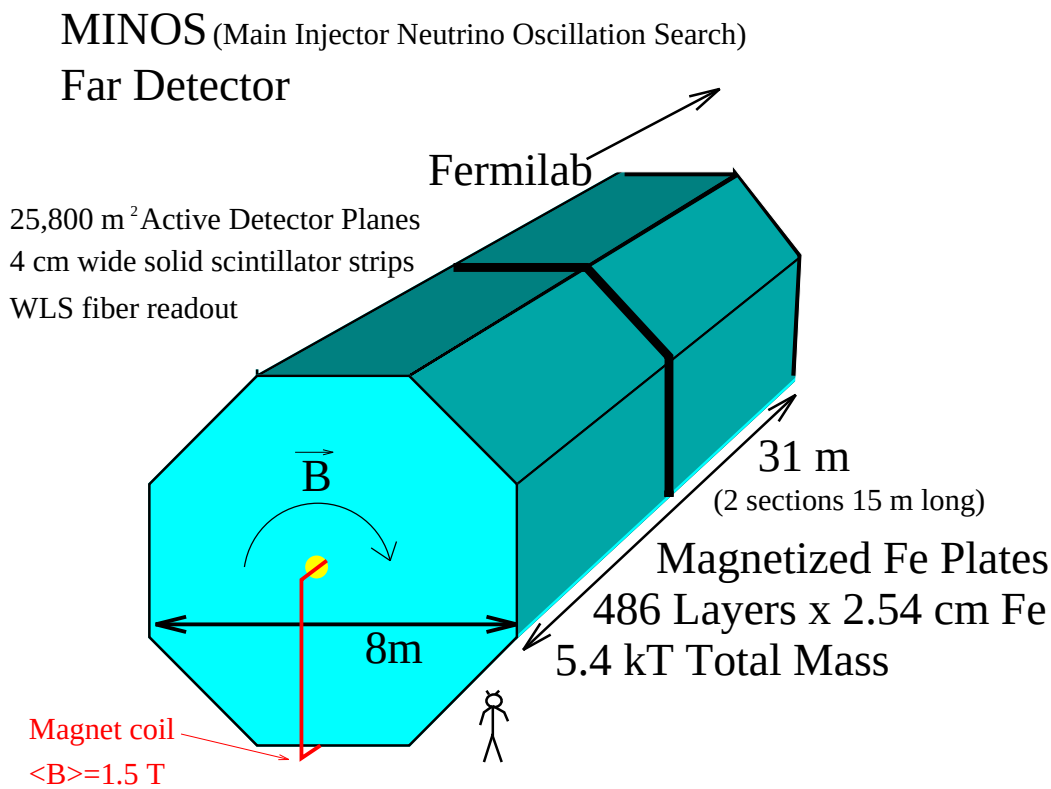

Figure 3.9: Sketch of the MINOS far detector.

Each scintillator plane is made up of 192 strips, each one 4 cm wide and up to 8 m long, depending on their location in the plane. The orientation of the strips alternates by $\pm 90°$ in successive planes. Each scintillator strip has a wavelength shifting fiber imbedded in it to capture, wavelength shift, and transport the light to the two ends. Both ends of each fiber are coupled through clear fibers and multiplexing boxes to multipixel photomultiplier tubes. Eight different fibers, from eight strips spaced roughly 1 m apart on the detector, are coupled to each pixel. The resultant 8-fold ambiguity can be resolved in software by utilizing the fact that the exact arrangement of which fiber is coupled to which pixel is somewhat different at the two strip ends. In addition, we will use timing and pulse height information from adjoining planes to provide independent ambiguity resolution.

The MINOS far detector will be located in a new cavern, to be excavated in 1999-2000, next to the cavern where the Soudan 2 detector is already operating. The MINOS cavern will

be oriented so that its axis points toward Fermilab. A perspective view of the two caverns and their access shafts and corridors is shown in Figure 3.10.

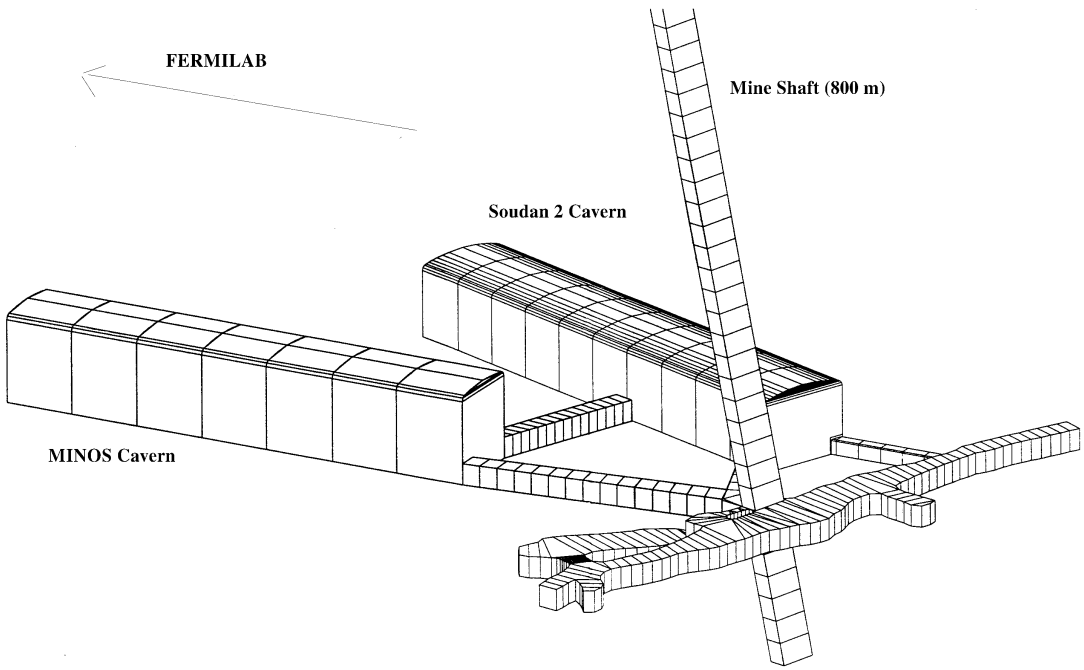

Figure 3.10: Sketch of the MINOS and Soudan 2 caverns in the Soudan Underground Mine State Park in northern Minnesota.

The MINOS Collaboration has adopted a baseline design of the far detector based on the results of three years of highly focused R&D work[10]. This development program has included extensive laboratory tests of different active detector technologies, test beam work, Monte Carlo simulations of reactions of interest to MINOS, and evaluation of the costs of various options. We believe that this baseline design represents the best experimental approach, in light of the current knowledge of neutrino oscillation physics, and also offers a high probability of being able to react effectively to potential future physics developments.

The existing Soudan 2 detector, described in Chapter 10, is viewed by the Collaboration as an integral part of the MINOS experiment. At the beginning of the run it will provide us with an opportunity to study neutrino interactions in Minnesota with a well understood detector. Results from that detector will be available immediately, in real time. Subsequently, Soudan 2 will offer complementary capabilities to the main MINOS far detector: very fine granularity, but lower mass. Soudan 2 should be able to identify examples of exclusive neutrino interaction channels, for example quasi-elastic τ-lepton production and its subsequent

decay through the $\tau \to e\nu\nu$ mode.

The baseline design of the MINOS detector has two supermodules with a total mass of 5.4 kt. We believe that the rather generous contingency allowed, together with our scope reserve, may permit us eventually to enlarge the detector while remaining within the financial constraints imposed on the total MINOS detector cost. This issue should be reexamined roughly two years from now when the costs are better understood. If financial considerations allow it, we might then build another supermodule or augment the detector with alternative instrumentation. The actual course of action would be influenced by future developments in physics and technology. One especially interesting option is a hybrid emulsion detector with a mass of a few hundred tons which would detect τ's by their decay kinks on an event by event basis. We are currently in the midst of an active R&D program to investigate this option, as is described in Chapter 11. This option is not a part of the present baseline design; its only impact on our current planning is that we plan to leave open the upstream 10 m of the MINOS cavern, reserving that space for the subsequent addition of a possible emulsion detector to complement MINOS.

3.7 MINOS physics capabilities

The combination of the NuMI beam and the MINOS detectors, whose characteristics are summarized in the previous three sections, has been designed to provide an optimum tool to search for and to study neutrino oscillations. But the design has also been guided by our belief that nonaccelerator issues will still be of great interest in 2002 when MINOS becomes operational. This dual capability of MINOS is described in the next two Sections.

3.7.1 Accelerator neutrino physics

In this Section we shall describe MINOS physics capabilities using Main Injector neutrinos. The potential measurements can be divided into three groups: statistical measurements, $\nu_\mu \to \nu_e$ identification, and study of exclusive τ decay channels. They all provide information about neutrino oscillations and will give us complementary and mutually reinforcing information should a positive signal be observed.

The statistical measurements can be viewed as providing four independent quantities, namely the rates and energy spectra for both neutral current (NC) and charged current (CC) reactions. In practice, the event identification for this study is actually made by classifying events as either "short" or "long," but we use the NC/CC nomenclature as being roughly equivalent. Both rate and energy measurements of CC events yield results which are independent of the mode of oscillation. Any mode of ν_μ oscillations will result in the depletion of ν_μ CC events, and the CC energy spectrum can be used to measure the oscillation parameters. Comparison of CC energy spectra at the near and far detectors allows us to determine the relative fraction and the energy spectrum of the "missing" events. The size of the depletion is related to $\sin^2(2\theta)$ and their mean energy provides a measure of Δm^2. Figure 3.11 displays this effect for two different sets of the oscillation parameters.

As the third statistical measurement, we choose to use the ratio NC/CC, rather than the rate of the NC events themselves. This ratio has the advantage that it does not require

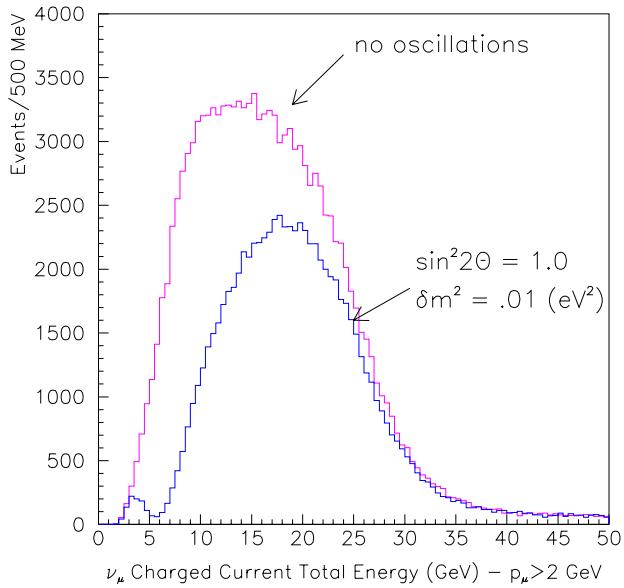

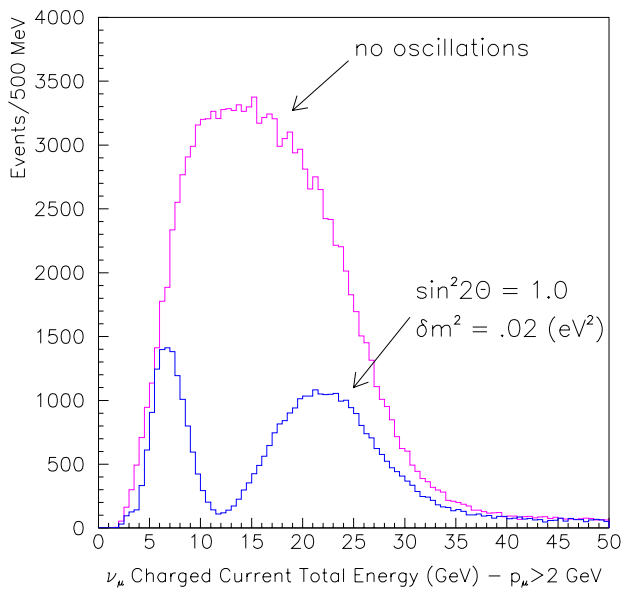

Figure 3.11: Energy spectrum of reconstructed ν_μ^{CC} events in the MINOS far detector in the case of no oscillations, compared to the spectra obtained for oscillations with $\Delta m^2 = 0.01$ eV^2 (top) and $\Delta m^2 = 0.02$ eV^2 (bottom). The high-energy WBB has been assumed, and the spectra have been smeared by expected detector resolution.

understanding of the relative fluxes at the near and far detectors and thus is less subject to systematic errors. It is quite sensitive to oscillations because, not only are the CC events depleted, but the NC events are enhanced, since most of the ν_τ and all of the ν_e events created through oscillations will add to the NC category.

The NC energy spectrum is also quite sensitive to oscillations. Whereas the true NC events will give a spectrum peaked at low energies, both ν_e and ν_τ CC events will tend to populate preferentially the higher energy region. This effect is illustrated in Figure 3.12. The power of the NC-event rate and energy spectrum measurement has been demonstrated by the CCFR experiment[11], which has been able to set a limit on $\sin^2(2\theta)$ of 2.7×10^{-3} (1.9×10^{-3}) for $\nu_\mu \to \nu_\tau$ ($\nu_\mu \to \nu_e$) oscillations in the region of Δm^2 corresponding to their maximum sensitivity. The NC measurements, when combined with the CC measurements, are able to identify the relative contributions of the different oscillation modes.

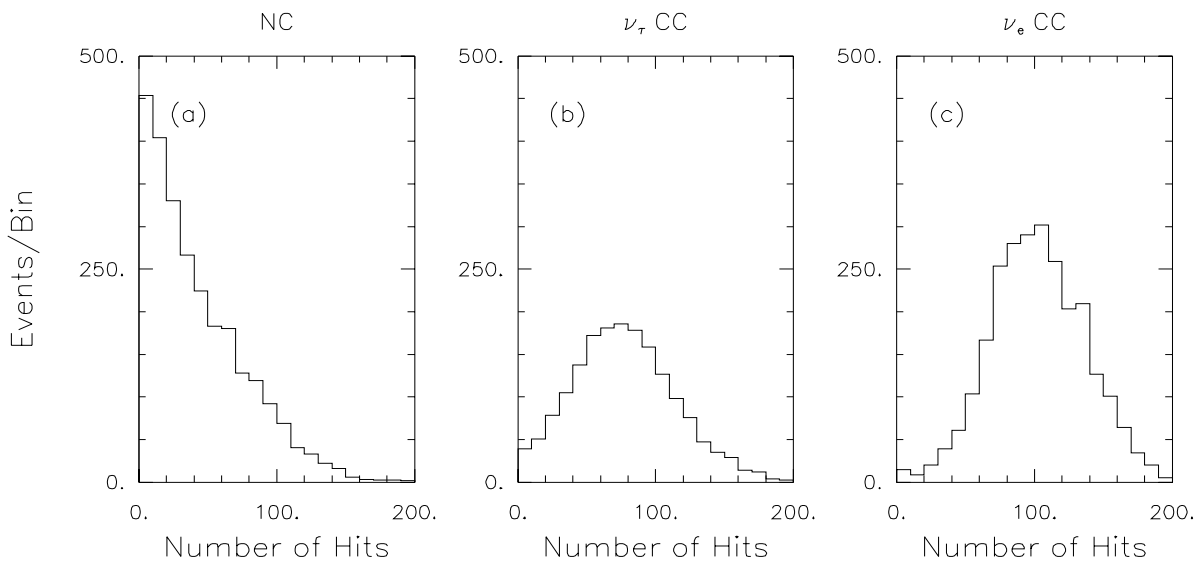

Figure 3.12: Effect of neutrino oscillations on the energy spectra of events with neutral current topologies in the MINOS far detector. The simulation used a 10 kt-year exposure with the high-energy beam in a detector with 2-cm thick steel planes and 2-cm wide scintillator strips. NC events were selected with a 20-plane length cut. The number of hit strips is used as a measure of event energy. The spectrum for true NC events is shown in (a). Oscillations with $\Delta m^2 = 0.01$ eV^2 and $\sin^2(2\theta) = 1.0$ for $\nu_\mu \to \nu_\tau$ and $\nu_\mu \to \nu_e$ produce the spectra (from ν_τ and ν_e CC events) shown in (b) and (c) respectively.

MINOS has excellent capability to distinguish ν_μ and ν_e CC events from NC events based on the shapes of hadronic and electromagnetic showers. The ν_e CC events will deposit most of their energy early in the shower, and the transverse width of the shower will be significantly narrower than for the hadronic shower of the NC events, which constitute the main background. The CCFR experiment[12] has already demonstrated that at high energies one can identify the ν_e CC events by the longitudinal shape alone, even with 10 cm thick iron plates. Our sensitivity to $\nu_\mu \to \nu_e$ oscillations using this method will be limited mainly by the statistical fluctuations in the number of ν_e CC events expected in the far detector

due to the ν_e component in the beam.

The MINOS sensitivities obtained by different methods, at the 90% confidence level, for both $\nu_\mu \rightarrow \nu_\tau$ and $\nu_\mu \rightarrow \nu_e$ are shown in Figure 3.13. The limit curves shown correspond to a 10 kt-yr (before fiducial cuts) exposure of the far detector in the high-energy wide-band beam, using realistic fiducial volume cuts. The assumed 1% systematic error limits the sensitivity of the near-far rate comparison test.

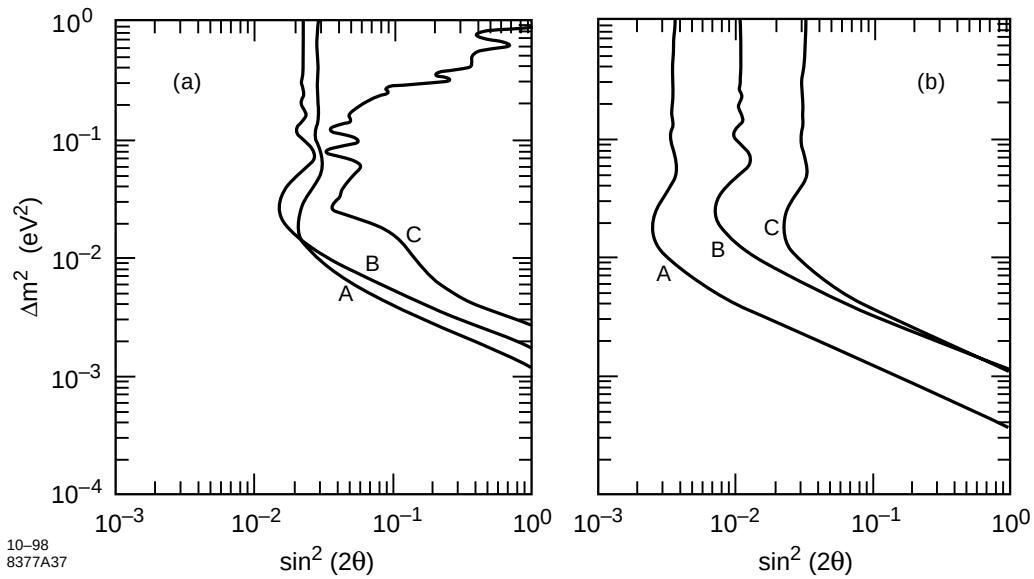

Figure 3.13: 90% confidence level limits on neutrino oscillation parameters which would be established by MINOS with 10 kt-years in the absence of oscillations, using the high energy wide band beam. The A, B and C curves show limits obtained from different oscillation tests. (a) $\nu_\mu \rightarrow \nu_\tau$ limits, where curve A is for the near-far event rate comparison, B is for the NC/CC ratio test, and C is for the CC-event energy test. (b) $\nu_\mu \rightarrow \nu_e$ limits, where curve A is for the electron appearance test, B is for the NC/CC ratio test, and C is for the near-far event rate comparison.

Our studies to date indicate that we should be able to identify, with a signal to noise ratio of better than 1:1, several τ exclusive decay modes. For example, for the parameters Δm^2 =0.01 eV^2 and $\sin^2(2\theta) = 1.0$ we would obtain a 7 σ effect for the $\tau \rightarrow \pi(K)\nu$ mode. For the modes $\tau \rightarrow e\nu\nu$ and $\tau \rightarrow$ hadrons(s) + π°(s) we can do even better, but there is some confusion in these channels with the ν_e CC interactions, and thus there is a mode ambiguity. Our capability for tau identification has been summarized in an internal report prepared for the Fermilab PAC[13].

The reach of MINOS can be extended to lower values of Δm^2 by using the lower energy PH2(medium) and PH2(low) beam configurations. Our sensitivity using the PH2(low) beam and the CC ν_μ disappearance test is shown in Figure 3.14.

In addition, we can perform a number of independent measurements with the Soudan 2 detector. Those have been described in detail in the original MINOS proposal[2] and are summarized in Chapter 10.

Finally, if our initial physics results justify it, MINOS has the capability of additional

running in the NBB configuration. These studies would provide a number of independent measurements on such issues as the existence of oscillations, the values of oscillation parameters, and the relative contributions of different oscillation modes. The quality of these results would be comparable to those obtained from the WBB running, but the systematics would be very different.

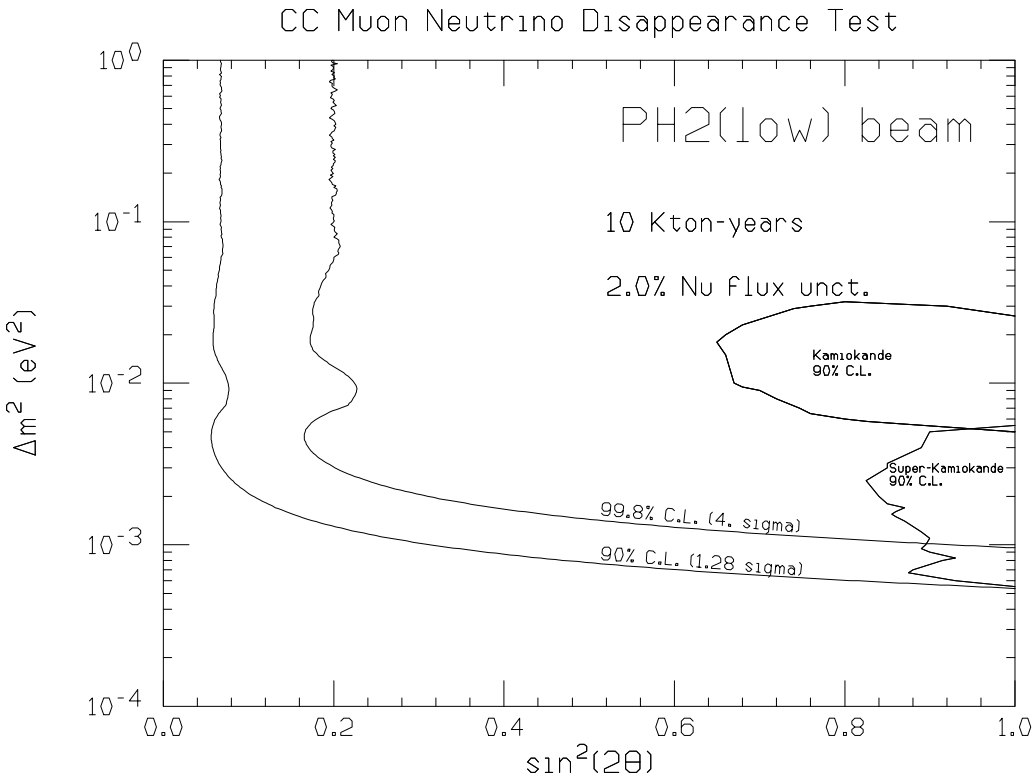

Figure 3.14: Sensitivity of the ν_μ disappearance test (90% CL limits and 4σ contour) for a 10 kt-yr exposure in the low energy PH2(low) neutrino beam.

3.7.2 Nonaccelerator phenomena

The MINOS detector will be the first large underground detector with a magnetic field. Thus it will be able to provide new information on a variety of nonaccelerator physics issues even though it will follow several years after other big underground detectors, notably Super-Kamiokande and MACRO[14].

The issue of atmospheric neutrinos is one where MINOS could make significant contributions. At the present time the two sets of measurements from Super-Kamiokande that are relevant to the neutrino oscillation hypothesis, namely the μ/e ratio-of-ratios R (Section 2.3.3.1) and the L/E distribution, are on the verge of being inconsistent with each other; the R value appears to require a higher value of Δm^2 than the L/E distribution. Furthermore the parameter region indicated by the Super-Kamiokande data is barely consistent with that derived from Kamiokande data analysis. The ability of MINOS to measure the energy of the muon, and hence of the neutrino initiating a CC event, will allow us to under-

stand the behaviors of L/E and the R value (as a function of energy) in more detail than is possible today. In addition, MINOS will provide complementary information about the sign of the muon. The ability to study atmospheric neutrinos should allow MINOS to extend its Δm^2 reach to values near 10^{-4} eV^2. We are currently studying the potential capabilities of our detector in this area.

Another area where there is a lack of good understanding today is upward going cosmic ray muons. The conventional explanation for these muons is that they are produced by upward going neutrinos interacting in the earth beneath the detector. Thus their rate and energy spectrum is sensitive to neutrino oscillations. The current status is somewhat murky. The measured rate from MACRO[15] is lower than predicted from the conventional cosmic ray neutrino calculations (as would be expected for $\nu_\mu \rightarrow \nu_e$ or $\nu_\mu \rightarrow \nu_\tau$ oscillations) but the observed zenith angle distribution is anomalous. The data from Super-Kamiokande and Kamiokande[16] on this topic are consistent with the oscillation hypothesis but do not provide any strong constraint on oscillation parameters. There is very little information on the energy or charge distributions of these muons (only the ratio of stopping to through-going muons has been measured). MINOS will provide unique information in both of these areas.

MINOS will also be able to study a number of other astrophysics issues. Some examples are cosmic ray muon studies, searches for point sources and large scale anisotropies, and searches for new exotic particles. Our capabilities in this area are described in more detail in the MINOS Proposal[2] and in its Addendum[17].

3.8 Future MINOS options

The baseline NuMI/MINOS project consists of the parabolic horn neutrino beam (which can be tuned to produce a wide range of neutrino energies), the associated conventional facility construction, the near detector cavern with the MINOS near detector, the new cavern in the Soudan mine, and the 5.4 kt iron calorimeter MINOS far detector. We believe that this combination will allow us to do excellent neutrino physics and to address in a definitive way many of the current unresolved issues in neutrino oscillation physics.

On the other hand, neither physics nor technology will remain stationary during the four year period required to construct the NuMI/MINOS facility. In light of that, and in light of the considerable investment required to construct the experiment, we feel it is appropriate for us to start thinking now about the possible evolution of the program in the future. This is consistent with Recommendation 4 of the Sciulli Subpanel[4] and the advice from the Fermilab PAC. This evolution might suggest future modifications of the baseline design or additions to it. In this final section of the Overview Chapter, we briefly mention some of the possibilities that might become attractive in the future. Several of them have been already alluded to in previous discussion.

A very attractive possibility would be to incorporate in the detector an ability to identify τ's on an event by event basis. The best way to accomplish this with today's technology (or small extrapolations from it) is with a hybrid emulsion detector. Our effort in this area is described in Chapter 11. Should this look feasible, attractive and cost effective, as a result of our R&D effort and other developments around the world, we would propose to build an

emulsion-based detector as an addition to the 5.4 kt calorimeter. We are therefore proposing to reserve space for such an addition in the upstream part of the new Soudan cavern. This location would allow the MINOS detector to be used as a muon spectrometer for the events produced in the emulsion detector.

As described in Section 2.3.3.4, it is quite likely that the atmospheric neutrino anomaly can be explained by $\nu_\mu \rightarrow \nu_\tau$ oscillations. However, in this scenario there is still a large uncertainly in the value of Δm^2 responsible for the oscillations. The zenith angle distributions from Super-Kamiokande suggest that this value could be 10^{-3} eV^2 or even lower. In that case, a lower energy beam would be more effective for studying the oscillations, given the 730 km distance from Fermilab to Soudan. The NuMI beam facility has been designed so that the beam elements can be configured to give much higher fluxes of low energy neutrinos.

Another possible beam alteration is running in the narrow band beam (NBB) configuration. Such a modification would make sense if we knew the oscillation parameters with reasonable certainty. In that case, NBB running would allow us to provide independent confirmation of an oscillation hypothesis and to perform measurements of the oscillation mode and parameters in a different, and perhaps a better, way. The NBB configuration has been designed and the changeover from the baseline beam configuration could be made in a relatively straightforward way if the physics situation should warrant it.

Another potential future modification would be an upgrade of the MINOS far detector by surrounding it with a veto shield. Such a shield would improve the quality of nonaccelerator physics measurements by providing good identification of externally produced muons and a much longer time base to determine the direction of tracks which enter or leave the main MINOS detector. The latter would be important in obtaining a clean sample of upward going muons and would also clarify the nature of events occurring near the edges of the detector.

Chapter 3 References

[1] C. Athanassopoulos *et al.*, Phys. Rev. Lett. **75**, 2650 (1995); J.E. Hill, Phys. Rev. Lett. **75**, 2654 (1995).

[2] The MINOS Collaboration, "P-875: A Long-baseline Neutrino Oscillation Experiment at Fermilab," February 1995, Fermilab report NuMI-L-63.

[3] The MINOS Collaboration, "MINOS Physics Goals and Experimental Requirements," January 1997, Fermilab report NuMI-L-229.

[4] "Report of the HEPAP Subpanel on Accelerator-Based Neutrino Oscillation Experiments," September 1995, DOE Office of Scientific and Technical Information Report No. DOE/ER-0662.

[5] The MINOS Collaboration, "Neutrino Oscillation Physics at Fermilab: The NuMI-MINOS Project," May 11, 1998, Fermilab report NuMI-L-375.

[6] The MINOS Collaboration, "MINOS Progress Report to the Fermilab PAC," October 1997, Fermilab report NuMI-L-300.

[7] W.W.M. Allison *et al.*, Phys. Lett. **391A**, 491 (1997); W.W.M. Allison *et al.*, Nucl. Instrum. and Methods **A376**, 36 (1996) and **A381** 385 (1996); S.M. Kasahara *et al.*, Phys. Rev **D55**, 5282 (1997); H.M. Gallagher, "Neutrino Oscillation Searches with the Soudan 2 Detector," University of Minnesota Ph.D. thesis, 1996.

[8] J. Hylen *et al.*, "Conceptual Design for the Technical Components of the Neutrino Beam for the Main Injector (NuMI)," September 1997, Fermilab-TM-2018.

[9] The Fermilab NuMI Group, "NuMI Facility Technical Design Report," October 1998, Fermilab report NuMI-346.

[10] The MINOS Collaboration, "MINOS Experiment R&D Plan: FY 1996-1998," June 1996, Fermilab report NuMI-L-184.

[11] K.S. McFarland *et al.*, Phys. Rev. Lett. **75**, 3993 (1995).

[12] A. Romosan *et al.*, Phys. Rev. Lett. **78**, 2912 (1997).

[13] The MINOS Collaboration, "Status Report on τ Identification in MINOS," January 1997, Fermilab report NuMI-L-228.

[14] F. Ronga, "Upgoing Muons in MACRO," Proceedings of the 25th International Cosmic ray Conference, Durban, South Africa, July 1997.

[15] S. Ahlen *et al.*, Phys. Lett. **B357**, 481 (1995).

[16] T. Kajita, "Atmospheric neutrino results from Super-Kamiokande and Kamiokande – Evidence for neutrino oscillations," talk presented at the Neutrino 98 Conference, Takayama, Japan, June 1998; S. Hatakeyama *et al.*, Phys. Rev. Lett. **81**, 2016 (1998).

[17] The MINOS Collaboration, "Addendum to P-875: A Long-baseline Neutrino Oscillation Experiment at Fermilab," April 1995, Fermilab report NuMI-L-79.